ELSEVIER

Chemical Geology 239 (2007) 182–198

CHEMICAL GEOLOGY
INCLUDING
ISOTOPE GEOSCIENCE

www.elsevier.com/locate/chemgeo

Transportation of H_2O beneath the Japan arcs and its implications for global water circulation

Hikaru Iwamori

Department of Earth and Planetary Sciences, University of Tokyo, 7-3-1 Hongo, Tokyo 113-0033, Japan

Accepted 18 August 2006

Editor: S.L. Goldstein

Abstract

In order to understand the transportation and circulation of H_2O in subduction zones, geological and seismological observations and the corresponding quantitative modeling are reviewed and consolidated, with a special emphasis on the Japan arcs. The Japan arcs are ideal for such a study in that (1) they are very active magmatically and seismically with abundant high-quality observations, and (2) subduction parameters change significantly along the Japan arcs allowing one to investigate how the variations of 'input' parameters affect the resultant structures and processes. First, numerical models for the transportation of H_2O and melting are introduced. The generation and migration of aqueous fluid, its interaction with the convecting solid, and melting are considered, based on the realistic phase relationships of the peridotitic and basaltic systems. Application of the models to the Japan arcs and comparison between the model results and the observations (distribution of volcanoes and seismic structures) along the Japan arcs are then discussed. The three cases from the NE, central and SW Japan arcs clarify the following points. First, an aqueous fluid released from the subducting oceanic crust forms a serpentinite layer in the mantle wedge just above the subducting slab, maintaining a condition close to equilibrium in terms of hydration–dehydration reactions during aqueous fluid migration. Second, most of the H_2O is subducted to a depth where serpentine and chlorite in the serpentinite layer break down. This depth depends on the thermal structure of the slab, and is greater for the older plate beneath the Japan arcs. As a consequence, aqueous fluid and melt are, in general, not supplied straight upward to the volcanic front. This result is rather different from the conventional view. Finally, based on the understanding obtained from the Japan arcs, the global budget and circulation of H_2O are discussed. Even after the completion of dehydration of major hydrous mineral phases in the subducting materials, especially at the base of the mantle wedge just above the subducting slab, nominally anhydrous phases of the upper mantle assemblage (i.e., olivine, pyroxenes, garnet) can carry a significant amount of H_2O (1.1×10^{11} to 7.8×10^{11} kg yr^{-1}) into the deep mantle. The minimum estimate is comparable to the outflow of H_2O from the mantle at mid-ocean ridges and hotspots, while the maximum estimate greatly exceeds it. The large estimated range is mainly due to the uncertainty of the maximum H_2O contents in the nominally anhydrous minerals of the upper mantle, which controls the net influx of H_2O into the deep mantle through subduction zones.Water; Subduction; Magmatism; Global circulation

Keywords: Water; Subduction; Magmatism; Global circulation

1. Introduction

Quantifying the transportation of H_2O into the mantle during subduction is key to understanding many of the distinct processes within the Earth. For example, it is

E-mail address: hikaru@eps.s.u-tokyo.ac.jp.

0009-2541/$ - see front matter © 2006 Elsevier B.V. All rights reserved.
doi:10.1016/j.chemgeo.2006.08.011

important for understanding the origin of magmatism and metamorphism in subduction zones, which are likely to be related to the growth of continents and orogeny on geologic time scales. It is also important for understanding the global dynamics, since H_2O affects greatly the physical properties of the mantle, such as phase relations, density and viscosity, which then affect mantle convection and the global mass–energy cycle. In this context, subduction zones are important as they deliver H_2O (and other materials and energy) into the mantle, and the processes attending subduction greatly control the processes stated above through the amount of H_2O transported into the mantle.

Within the subducting slab, pressure and temperature increase as the slab subducts. This causes the dehydration of H_2O-bearing minerals and results in the generation of aqueous fluid. The aqueous fluid is thought to ascend, due to buoyancy, along solid grain boundaries or through cracks. This results in variable extents of chemical reaction with the mantle wedge and may involve melting of the wedge (e.g., Davies and Stevenson, 1992; Iwamori, 1998; Arcay et al., 2005), as is schematically shown in Fig. 1. Therefore, in order to understand the subduction zone processes described above, a spectrum of physical and chemical aspects, such as thermal and flow structures of solid and fluid that chemically interact with each other, need to be estimated simultaneously and quantitatively.

Recent studies detailing geological and seismological observations in subduction zone settings, together with the corresponding quantitative modeling, allow us to deduce the controlling factors of the fluid processes in subduction zones. The Japan arcs are ideal for such a study in several aspects. Along the Japan arcs, the subduction parameters (e.g., age and velocity of the subducting slab) change significantly as described below, such that one can test how the variations of 'input' parameters affect the resultant structures and processes in the subduction zone by comparing the observations and model results. The Japan arcs are very active magmatically and seismically, and the significant number of high-quality observations, especially for the seismic structures, e.g., high-resolution body-wave tomography (Zhao et al., 1992; Nakajima et al., 2001), and analyses of the distribution of volcanoes and the corresponding modeling of mantle processes (e.g., Kondo et al., 1998; Iwamori, 2000; Tamura et al., 2002; Honda and Yoshida, 2005) make the Japan arcs a perfect natural laboratory to study subduction processes. The structures and processes that are thought to be related to the presence of aqueous fluids or hydrous minerals have also been discussed extensively. Specifically, the distribution of aqueous fluid and melt (e.g., Iwamori and Zhao, 2000; Nakajima et al., 2001; Nakajima et al., 2005), the existence of serpentine in the mantle wedge (Kamiya and Kobayashi, 2000) and dehydration within and around the subducting slab (e.g., Wyss et al., 2001; Yamasaki and Seno, 2003).

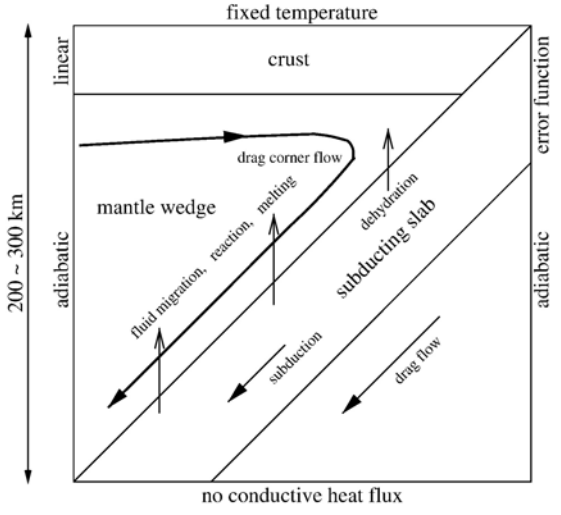

Fig. 1. Schematic figure showing a model of transportation of H_2O and melting in subduction zones. The boundary conditions of temperature for the model are shown along the outline of the box.

The main aim of this paper is to review and consolidate the observations and numerical models beneath the Japan arcs in order to gain a comprehensive view of the transportation and circulation of H_2O in subduction zones. The model results are compared with observations such as distribution of volcanoes and seismic structures along the Japan arcs, in which the age of the subducting slab is found to be a key factor. Finally, based on the understanding obtained from the Japan arcs, the global budget and circulation of H_2O will be discussed.

2. Tectonic setting of the Japan arcs

Two oceanic plates, the Pacific and the Philippine Sea plates, subduct beneath the Japan arcs (Fig. 2). The Pacific plate subducts along the Kuril and Japan trenches beneath Hokkaido, northeast Japan, central Japan, and Izu–Ogasawara with the subduction velocity of 8 to 10 cm/yr to the northwest (e.g., DeMets et al., 1990; Bird, 2003). The age of the Pacific plate in these regions reaches 130 Ma. The Philippine Sea plate subducts at the Sagami and Nankai troughs beneath central Japan, Chugoku, Shikoku, Kyushu, and Ryukyu with a subduction velocity of 3 to 5 cm/yr to the northwest (e.g., Seno et al., 1993; Bird, 2003). The Philippine Sea plate can be

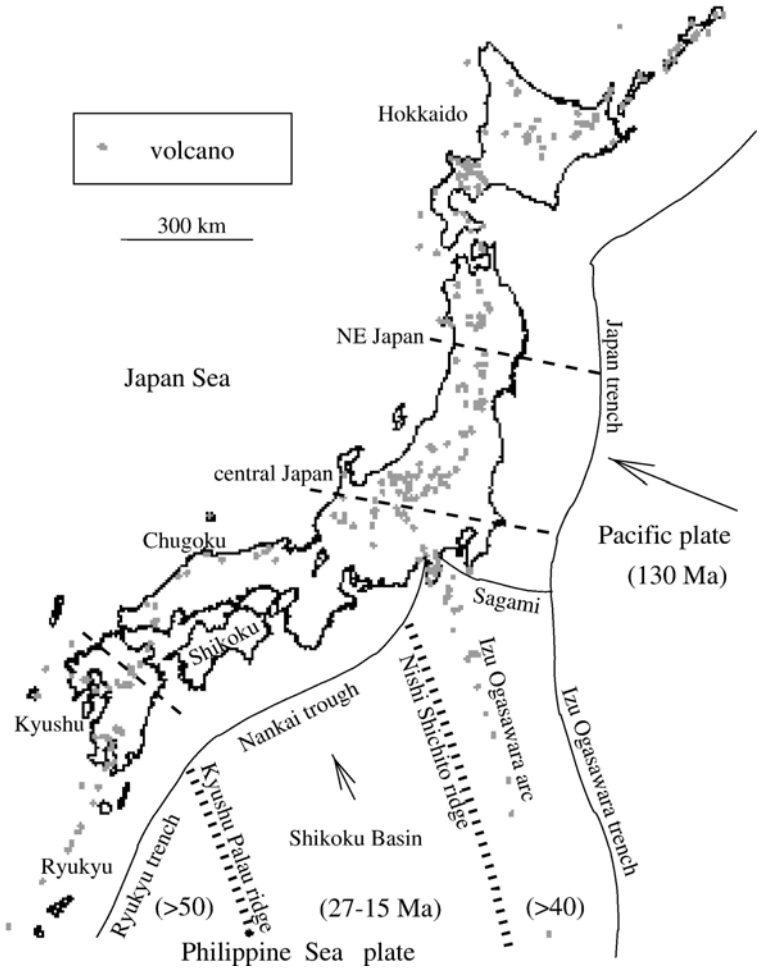

Fig. 2. Tectonic setting around the Japan arcs. Broken lines correspond to across-arc sections of the models for NE Japan, central Japan and Kyushu.

divided into three north-south trending regions, according to the formation age (Fig. 2): (i) the eastern part including the Izu–Ogasawara arc formed before 40 Ma; (ii) the central part, the Shikoku basin, which was formed as a backarc basin from 27 to 15 Ma (Okino et al., 1994); and (iii) the western part consisting of several old ridges and basins older than 50 Ma (e.g., Tokuyama, 1995). The eastern part subducts at the Sagami and Nankai troughs, causing a collision of the central Japan arc and the Izu–Ogasawara arc. A former spreading axis exists in the central part, the Shikoku basin, and subducts at the Nankai trough, between the Kii peninsula and Shikoku. The old western part subducts beneath Kyushu and the Ryukyu arc (Fig. 2).

The geometry of the subducted Pacific plate has been well constrained from the distribution of hypocenters and tomographic studies (e.g., Zhao and Hasegawa, 1993) which suggest that the leading edge reaches a depth of 500 km or more beneath the Japan Sea. The geometry of the subducted Philippine Sea plate beneath central Japan is less well constrained when compared with that of the Pacific plate, but has been deduced also from the distribution of hypocenters, analyses of converted waves, and tomographic studies (e.g., Iidaka et al., 1990; Ishida, 1992; Nakamura et al., 2002; Matsubara et al., 2005). These studies suggest that (i) the leading edge reaches a depth of 60–100 km beneath the eastern part of central Japan (north of Kanto region), overlapping the subducted Pacific plate (Fig. 3), (ii) an aseismic slab exists beneath the north of the Izu peninsula, where the arc–arc collision occurs, and (iii) beneath the western part of central Japan (Tokai region), the slab extends northwards from the Nankai trough to a depth of 50–60 km with a shallow subduction angle and then kinks to a deeper mantle with a steep angle (nearly vertical) around 36° in latitude.

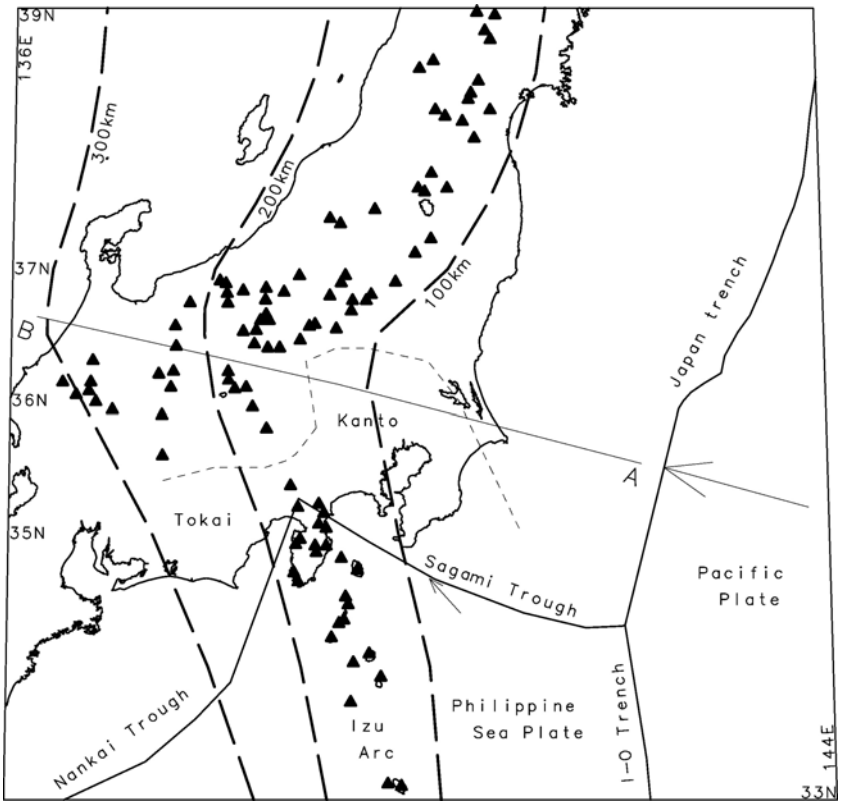

Fig. 3. Map showing the distribution of active volcanoes (solid triangles) and the plate configurations with the depth contour of the upper surface of the Wadati–Benioff zone of the subducting Pacific plate (thick broken lines), and the 'seismic' northern limit of the subducted Philippine Sea plate beneath the Kanto and Tokai regions (thin broken lines). 'I–O trench' indicates the Izu–Ogasawara trench. Across-arc section along the solid line A–B is modeled for transportation and melting beneath central Japan as is shown in Fig. 6b.

The subducted Philippine Sea plate, corresponding to the young Shikoku basin beneath southwest Japan (Shikoku, Chugoku, and northern Kyushu), is also confirmed by the seismicity associated with subduction, which extends over a relatively short distance from the trench, to ~150 km in the horizontal distance beneath northern Shikoku. An aseismic slab beneath Chugoku is suggested based on the analysis of ScS-waves and their conversion to P-waves (Nakanishi, 1980). This is explained by rapid thermal assimilation of the subducted young Shikoku basin, which becomes aseismic within a short distance. The subduction angle is ~15 degrees, possibly reflecting the young buoyant nature of the Shikoku basin, whereas the subducted Philippine Sea plate is kinked beneath western Shikoku and northern Kyushu with a steeper subduction angle (~45°) to the west.

In Fig. 2, gray dots show the location of Quaternary volcanoes along the Japan arcs. The volcanoes are aligned in general parallel to the trenches and the troughs, forming volcanic chains. However, the spatial details of the alignment along the arcs are not constrained. In northeast Japan, alignment parallel to the trench is recognized along the volcanic front, whereas the volcanoes (between 0 and 14 Ma) on the backarc side form several clusters rather than a continuous chain (Kondo et al., 1998). In central Japan, the parallelism is violated as the volcanic chain significantly deflects towards the backarc side as is shown in Figs. 2 and 3 (Iwamori, 2000).

In the Chugoku district, southwest Japan, a volcanic zone aligned along the Japan Sea coast (Daisen volcanic zone dominated by andesitic magmatism) has been thought to be associated with subduction of the Philippine Sea plate, including the possibility of slab melting (e.g., Kimura et al., 2005). However, Iwamori (1991, 1992) discussed that the Daisen volcanic zone is a product of crustal melting induced by alkaline basaltic volcanism associated with the upwelling of mantle abundant in volatile and incompatible elements over the past 12 Ma. Similar alkaline basaltic volcanism, of non-island arc type, is recognized during the same period over a wide area, including the backarc side of northern Kyushu (e.g., basalts in Iki island and Kita-Matsuura), Korea and mainland China (Whitford-Stark, 1987). Considering its distinct and controversial origin, the

magmatism in the Chugoku district is excluded from the following arguments. The andesitic volcanism of the island–arc type, however, is recognized from the volcanic front in northern Kyushu to the Ryukyu arc (e.g., Kuju, Aso, and Sakurajima volcanoes), which again forms a volcanic chain parallel to the Ryukyu trench.

The along-arc variations in terms of seismicity and volcanism described above are associated with variable subduction parameters (velocity, angle, and age of the slab). This indicates that thermal and flow structures of solid and liquid within the slab and the mantle wedge have impacts on the geological processes observed. In the following, the numerical modeling that predicts these structures and processes is introduced. Then specific cases for the Japan arcs are discussed based on a comparison between the model results and the observations, including seismic structures and distribution of volcanoes.

3. Numerical model of transportation of H_2O

In order to assess the transportation of H_2O in subduction zones, it is necessary to incorporate the following aspects into the models: subduction of a slab, convection of the mantle wedge, phase equilibria of H_2O-bearing rocks for both subducted oceanic crust (basalt, sediment) and mantle wedge (peridotite), generation and migration of aqueous fluid and its reaction with the convecting solid (including melting; Fig. 1). Although a number of studies have discussed the relationship between dehydration and the thermal structure of the slab (e.g., van Kenken et al., 2002; Rüpke et al., 2004; Iwamori, 2004), there are only a few studies that also incorporate the generation and migration of the aqueous fluid and melt, which is essential since this modifies significantly the overall distribution and transportation of H_2O. Iwamori (1998) proposed a model integrating the processes above, with governing equations for mass–energy conservation and parameterized phase relationships for the H_2O-bearing systems. Arcay et al. (2005) similarly parameterized the phase relations and conducted a numerical simulation of thermal structure and fluid flow when subduction is initiated. Here we follow the model of Iwamori (1998) and Iwamori and Zhao (2000) in which the following simplifications and assumptions have been made: (i) convection of solid in the mantle wedge is assumed to be induced by the dragging of the subducting plate, and is assumed to be a steady flow with a constant viscosity; (ii) the aqueous fluid released from the subducting slab migrates via porous flow along solid grain boundaries maintaining local chemical equilibrium; and (iii) the melt, formed primarily at relatively shallow depths (<80 km) as will be shown, separates without chemical reaction from the solid above a critical melt fraction of 2% through cracks.

The assumption of constant viscosity in (i) is certainly a limitation and I will discuss the cases with variable viscosity later. Nakajima et al. (2005) analyzed theoretically the results of P- and S-wave tomography, together with attenuation, beneath NE Japan, to determine the fraction of liquids present and the pore geometry. They argue that liquids exist in tubes along solid grain boundaries within the main low-velocity zone beneath the backarc region above the subducting slab at ~90 km depth, whereas liquids exist in cracks at shallower levels (<60 km depths). Their conclusions justify the assumptions (ii) and (iii) described above.

To model the generation and migration of aqueous fluid and melt, phase relationships for the subducting slab and mantle wedge are required. The subducting slab consists of sediment, basaltic oceanic crust, and residual peridotite. The mantle wedge is thought to consist of peridotitic rocks. The H_2O-bearing phase relationships of these rock systems (e.g., Inoue, 1994; Bose and Ganguly, 1995; Hirose, 1997; Kawamoto and Holloway, 1997; Schmidt and Poli, 1998; Ono, 1998) have been parameterized numerically and are incorporated into the model including the maximum H_2O content in the solid (hereafter, referred to as $C^{H_2O}_{s,max}$) at a given P–T, including the melting conditions.

The phase relations of H_2O-peridotitic system and $C^{H_2O}_{s,max}$ up to 28 GPa are shown in Fig. 4a. The diagram is based on a compilation of the stability of hydrous phases in the MgO–SiO_2–H_2O, the MgO–Al_2O_3–SiO_2–H_2O, and KLB-1 peridotite systems (modified after Iwamori, 2004), including those of Kawamoto (2004) and Komabayashi et al. (2004). It should be stressed that the phase relation below 500 °C is extrapolated arbitrarily from those above 500 °C and has a large uncertainty, although it is not critical to the discussion in this study.

At relatively low pressure, below 5 GPa, and low temperatures, below 600–700 °C, serpentine and chlorite are stable and the peridotitic system can contain a maximum of ~7 wt.% H_2O in the solid phases. On the other hand, at temperatures above 600–700 °C, serpentine and chlorite in the system are unstable, and no major hydrous phase exists for the peridotitic system. At relatively high pressures of more than 10 GPa, phase A, phase E, superhydrous phase B and phase D are stable up to 1000 to 1200 °C where the peridotite can contain more than 10 wt.% H_2O.

Although $C^{H_2O}_{s,max}$ drastically decreases above the stability field of these major hydrous phases, the peridotites can still contain a significant amount of H_2O in the nominally anhydrous phases, especially in the transition zone. Wadsleyite and ringwoodite contain up to several wt.% H_2O, which decreases with temperature (e.g., Smyth, 1987; Inoue et al., 1995; Kawamoto et al., 1996; Kohlstedt et al., 1996; Litasov and Ohtani, 2003). Based on these results, the maximum H_2O content of the peridotitic rock in the transition zone is parameterized to decrease linearly with temperature from 2.0 wt.% on the practical H_2O-saturated solidus (corresponding to decomposition of phase E and superhydrous phase B) to 0 wt.% on the dry solidus (Fig. 4a).

The maximum H_2O contents of the upper and lower mantle shown in Fig. 4a and b are slightly modified from Iwamori (2004) to include recent data on the solubility of H_2O in nominally anhydrous minerals as described below. The maximum concentration of H_2O in olivine increases with pressure and reaches 0.12 wt.% H_2O at 13 GPa and 1100 °C (Kohlstedt et al., 1996), which is reevaluated to be 2 to 4 times greater based on a new calibration of IR spectrum (Bell and Rossman, 2003). The maximum concentration of H_2O in olivine increases with temperature at 0.3 GPa (Zhao et al., 2004), but is not directly constrained at high pressures. Pyroxenes can contain about 1000 ppm H_2O or even more than that of olivine, depending on P, T and composition, especially the Al content (e.g., Skogby, 1994; Rauch and Keppler, 2002; Mierdel and Keppler, 2004). Garnet and majorite can contain several 100 ppm to slightly more than 1000 ppm H_2O (e.g., Lu and Keppler, 1997; Withers et al., 1998; Bolfan-Casanova et al., 2000; Katayama et al., 2003). Using these H_2O solubility data and petrologically reasonable modal compositions, the maximum concentration of H_2O in the peridotitic rock of the upper mantle mineral assemblage has been estimated, which, however, shows a significant range reflecting the uncertainties stated above: e.g., 2760 ppm (Bolfan-Casanova, 2005) to 6500 ppm (Hirschmann et al., 2005) at 11.5 GPa.

The maximum concentrations of H_2O in the minerals that are stable at lower mantle conditions (i.e., Mg-/Ca-perovskite and magnesiowüstite, with or without Al and/or Fe) are also a matter of debate (see Bolfan-Casanova (2005) for the review and details). There are large variations due to experimental and analytical difficulties, resulting in the maximum concentration of H_2O in the lower mantle mineral assemblage varying from about 10 ppm (Bolfan-Casanova, 2005) to more than 1000 ppm (Murakami et al., 2002; Litasov et al., 2003).

Fig. 4b shows a model geotherm with the mantle potential temperature of 1300 °C as a representative geotherm (Turcotte and Schubert, 1982), and the maximum H_2O content along the geotherm. Although the geotherm passes mainly above the stability field of major hydrous phases, a significant amount of H_2O can be contained in the mantle along the geotherm, reflecting $C^{H_2O}_{s,max}$ of peridotites with the nominally anhydrous phases. This is shown by the broken and dotted lines in Fig. 4b. The broken line is based on the minimum estimate in the upper and lower mantle after Bolfan-Casanova (2005), whereas the dotted line corresponds to the maximum estimate after Hirschmann et al. (2005) for the upper mantle and Murakami et al. (2002) for the lower mantle (see the caption of Fig. 4 for the detail).

Table 1 shows the maximum H_2O contents of the upper mantle, transition zone and lower mantle along the geotherm, obtained by integrating $C^{H_2O}_{s,max}$ using the depth–density relation of PREM (Dziewonski and Anderson, 1981). These data suggest that the mantle has a potential storage of H_2O which is 4.6 to 12.5 times greater than the ocean mass; these results depend significantly on the estimation for the lower mantle as was discussed. Jambon and Zimmermann (1990) estimated the H_2O content of the bulk Earth to be 1300 ppm (with the lower and upper bounds of 550 and 1900 ppm, respectively) of which now 18% is in the ocean. In other words, the remaining 6.4×10^{21} kg of H_2O, or 4.5 times of the current ocean mass, is in the Earth's interior. In any case, if there is a communication between the surface water and the Earth's interior, the communication process, such as subduction of H_2O or degassing associated with magmatism at ridges, affects greatly the water budget and circulation of the Earth's system.

Fig. 5 shows $C^{H_2O}_{s,max}$ of the subducting basaltic oceanic crust. Unlike the peridotitic system, $C^{H_2O}_{s,max}$ in the basaltic system changes nearly continuously, due to (1) numerous reactions involving H_2O and (2) the effects of the solid solutions (Schmidt and Poli, 1998; Ono, 1998). The $C^{H_2O}_{s,max}$ decreases with an increase of pressure or temperature, especially between 1 and 2.5 GPa where amphibolite dehydrates and transforms into eclogite. Sedimentary rocks consisting of the top portion of the subducting slab exhibit a similar trend in terms of $C^{H_2O}_{s,max}$ (Ono, 1998). Therefore, in the current model, $C^{H_2O}_{s,max}$ of the subducting oceanic crust as a whole is represented as in Fig. 5 for the basaltic system.

According to the parameterized phase relationships, for a given set of temperature, pressure, and quantity of H_2O in the local system ($C^{H_2O}_{s,max}$), one can calculate the

quantity of aqueous fluid, melt, solid, and the H_2O content in each phase. Each phase then flows and reacts, which in turn determines the temperature and $C^{H_2O}_{s,max}$ for the next time step. This model is applied to the case with parameters that are appropriate for the Japan arcs and the boundary conditions shown in Fig. 1. The subducting plate is assumed to be a rigid slab with a constant subduction velocity and angle, which induces a corner flow in the mantle wedge owing to the drag force. Among the thermal boundary conditions shown in Fig. 1, the thermal structure of the subducting plate and the temperature profile given on the backarc boundary (left-hand side wall of the box of Fig. 1) are important. The former is constrained from the age of the subducting plate, and the latter is assumed to give a reasonable heat flux at the surface of the arc (see Iwamori (1998) for the details). In the next section, the model results are used to discuss the fluid processes beneath the Japan arcs (northeast Japan, central Japan, and southwest Japan).

4. Transportation of H_2O beneath the Japan arcs

4.1. Northeast Japan

Northeast Japan is characterized by subduction of the old Pacific plate (Fig. 2), where a clear Wadati–Benioff zone and active volcanism with a well-defined volcanic chain are observed. Northeast Japan is one of the best-studied area in terms of the seismic structures, including the tomographic image, of the subducting plate and the mantle wedge (e.g., Zhao et al., 1992; Nakajima et al., 2001), and is suitable for testing the model. Iwamori and Zhao (2000) applied the model described in the previous section to northeast Japan to predict thermal structure, distribution of fluids, and consequential seismic velocity structures, which have been compared with the P-wave tomographic images beneath the area. Here the predicted distribution of H_2O (H_2O contents in local bulk systems) is reproduced in Fig. 6a, which is schematically illustrated in Fig. 7a, with a special reference to the transportation agents and paths of H_2O.

For the subducted Pacific plate, the model calculation gives a relatively low temperature at the upper surface of the plate (e.g., ~610 °C at 200 km depth). In spite of the relatively cold environment, at depths between 30 and 80 km, a large amount of H_2O is released owing to the strongly pressure-dependent dehydration between 1 and 2.5 GPa of the hydrated oceanic crust (Fig. 5), which is assumed initially to contain 6 wt.% H_2O in hydrous phases such as amphibole, lawsonite, chlorite (Fig. 7a).

Aqueous fluid evolved from the subducting slab results in the formation of a serpentinite layer (i.e., a fully hydrated peridotite) in the mantle wedge just above the slab (a thin 'red' layer just above the slab in Fig. 6a). The serpentinite layer is subducted to a depth of ~150 km in the mantle wedge along the slab, where the temperature exceeds the stability fields of serpentine and chlorite. The aqueous fluid evolved from these minerals ascends upward owing to a strong density contrast. It reaches the central portion of the mantle wedge, where the temperature exceeds the hydrous solidus resulting in melt formation at ~80 km depth. In this case, dehydration and melting start from the backarc side, rather than beneath the volcanic front. Water is then transported both directly to the surface associated with melt segregation, and partly towards the trench side along the solid flow in amphibole and residual melt (Fig. 7a).

In this model, a constant viscosity has been assumed. If a temperature dependent viscosity is employed, the temperature distribution near the corner region of the mantle wedge is modified such that an inclined hot zone extends towards the corner, heating up the surface of the subducting slab more effectively than the case with a

Fig. 4. Phase relation of H_2O-saturated peridotite and the maximum content of H_2O in the solid phases ($C^{H_2O}_{s,max}$), which is based on compilation of the stability of hydrous phases in the MgO–SiO_2–H_2O, the MgO–Al_2O_3–SiO_2–H_2O, and KLB-1 peridotite systems (modified after Iwamori, 2004), including those of Kawamoto (2004) and Komabayashi et al. (2004). (a) phase assemblages of the H_2O-saturated peridotite (field no. 1 to 27) are shown on the right-hand side of the diagram. The abbreviations of the phases are as follows: ol=olivine; opx=orthopyroxene; cpx=clinopyroxene; pl=plagioclase; sp=spinel; gt=garnet; amp=amphibole; chl=chlorite; serp=serpentine; MgS=Mg–sursassite; A=phase A; chm=clinohumite; wd=wadsleyite; rg=ringwoodite; st=stishovite; mj=majorite; E=phase E; D=phase D; br=brucite; Ca-pv=Ca-perovskite; ak=akimotoite; sB=superhydrous phase B; pv=perovskite; pe=periclase (or magnesiowüstite); Al-phase=Al-rich phase. In the fields of no. 1, 14, 15, 21 and 26, which are above the stability fields of major hydrous phases, $C^{H_2O}_{s,max}$ is not zero as H_2O is contained in the nominally anhydrous phases (see text for the details), although it is not fully resolved by the gray scale used in the diagram. In the filed no. 1, the pressure dependence of $C^{H_2O}_{s,max}$ is described by $C^{H_2O}_{s,max}=aP^3+bP^2+cP$, ignoring the temperature dependence since it is poorly constrained at present. A minimum estimate based on Bolfan-Casanova (2005) gives $a=-0{:}875421$; $b=3{:}36700$; $c=317{:}054$, while the maximum estimate based on Hirschmann et al. (2005) gives $a=-4{:}59303$; $b=35{:}9208$; $c=759{:}557$. In the field no. 26, two bounding cases are considered: the minimum estimate of 10 ppm based on Bolfan-Casanova (2005), while the maximum estimate of 2100 ppm based on Murakami et al. (2005). (a) is drawn based on the minimum estimates for both the upper and lower mantle. (b) $C^{H_2O}_{s,max}$ along a representative geotherm (thick solid line), corresponding to that beneath an oceanic plate of 60 Ma with the mantle potential temperature of 1300 °C, is calculated based on (a). The broken line corresponds to the minimum estimate in the fields of no. 1 and 26, while the dotted line corresponds to the maximum estimate.

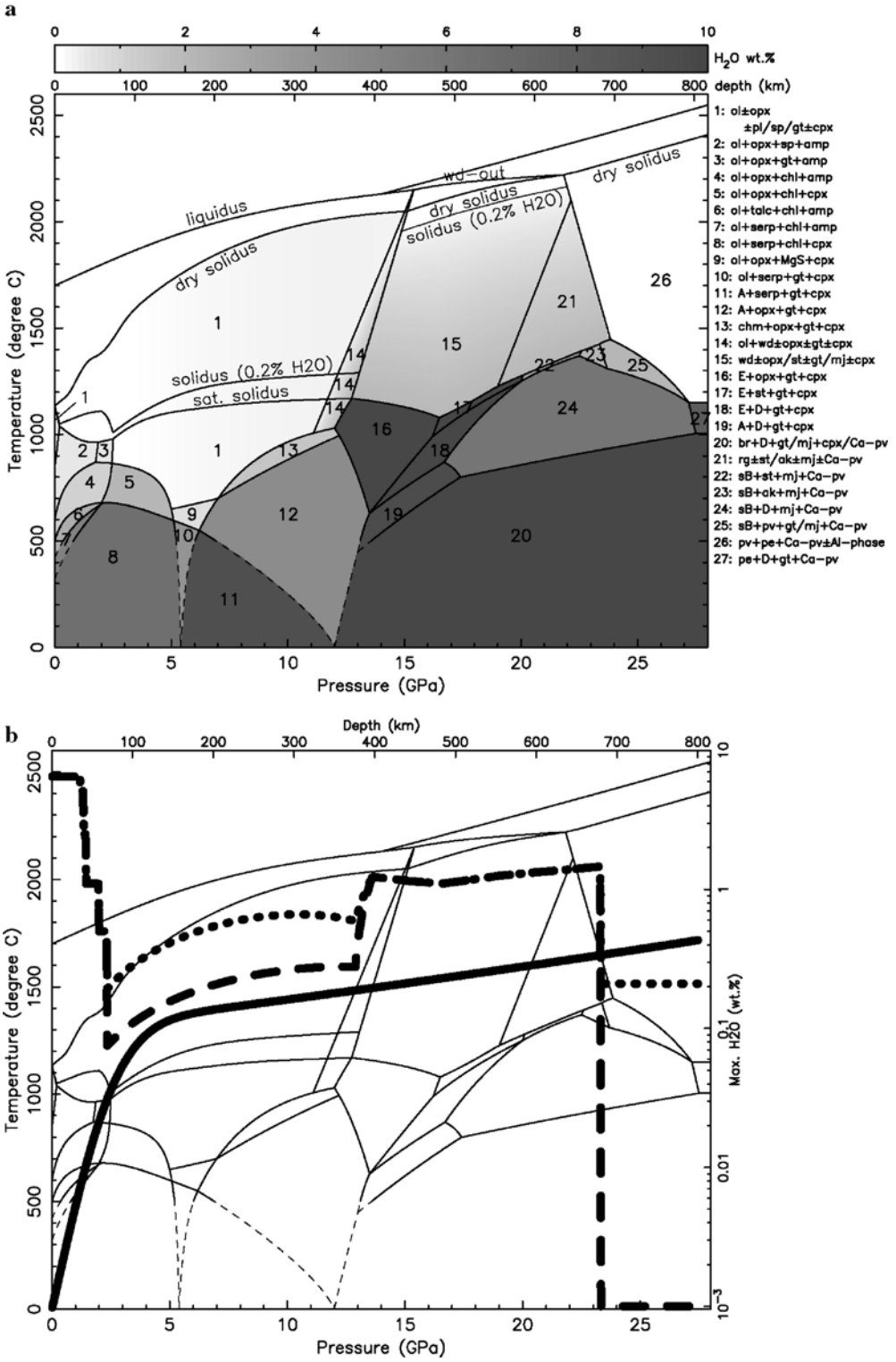
a
H2O wt.%
depth (km)
Temperature (degree C)
Pressure (GPa)
liquidus
dry solidus
wd-out
solidus (0.2% H2O)
sat. solidus
1: ol±opx ±pl/sp/gt±cpx
2: ol+opx+sp+amp
3: ol+opx+gt+amp
4: ol+opx+chl+amp
5: ol+opx+chl+cpx
6: ol+talc+chl+amp
7: ol+serp+chl+amp
8: ol+serp+chl+cpx
9: ol+opx+MgS+cpx
10: ol+serp+gt+cpx
11: A+serp+gt+cpx
12: A+opx+gt+cpx
13: chm+opx+gt+cpx
14: ol+wd±opx±gt±cpx
15: wd±opx/st±gt/mj±cpx
16: E+opx+gt+cpx
17: E+st+gt+cpx
18: E+D+gt+cpx
19: A+D+gt+cpx
20: br+D+gt/mj+cpx/Ca−pv
21: rg±st/ak±mj±Ca−pv
22: sB+st+mj+Ca−pv
23: sB+ak+mj+Ca−pv
24: sB+D+mj+Ca−pv
25: sB+pv+gt/mj+Ca−pv
26: pv+pe+Ca−pv±Al−phase
27: pe+D+gt+Ca−pv
b
Depth (km)
Temperature (degree C)
Pressure (GPa)
Max. H2O (wt.%)

Table 1
Maximum contents of H_2O of peridotites along the model geotherm shown in Fig. 4b

(unit)	Mass (10^{21} kg)	Max H_2O (10^{21} kg)	Max H_2O (wt.%)	Max H_2O (ocean mass)
Ocean	1.4	1.4	100	1.0
Upper mantle	615	4.2–5.8	0.68–0.95	3.0–4.2
Upper mantle*	615	1.1–2.8	0.18–0.45	0.79–2.0
Transition zone	415	5.4	1.3	3.8
Lower mantle	2955	0.03–6.2	0.001–0.21	0.02–4.4
Whole mantle	3985	9.6–17.5	0.24–0.44	6.9–12.5
Whole mantle*	3985	6.5–14.4	0.16–0.36	4.6–10.3

The masses of upper mantle (Moho to 410 km depth), transition zone (410–660 km), lower mantle (660–2886 km) are after Schubert et al. (2001), and the mass of ocean after McGovern and Schubert (1989). The ranges of the estimated contents correspond to the minimum and maximum estimates shown in Fig. 4b.
* The H_2O content at the region from 0 to ~3 GPa where $C_{s,max}^{H_2O}$ along the model geotherm exceeds ~2 wt.% with presence of serpentine and chlorite (Fig. 4b) has been ignored in the estimation, as it strongly depends on the near-surface structure of temperature.

constant viscosity (e.g., Furukawa, 1993). As a result, the depth at which serpentinite dehydrates is estimated to be shallower by 15 km, based on the temperature structure presented in Iwamori (2004). According to the results of van Kenken et al. (2002), in which the temperature–stress dependent viscosity is employed, the difference is estimated to be about 30 km, although a direct comparison with this study is not possible due to a difference in the mantle potential temperature (approximately 150° higher in van Kenken et al. (2002)). Therefore, the depth of major dehydration and position of the hydrous column have some uncertainties, yet the sequence and agents of H_2O transportation remain unchanged as in Fig. 7a.

Using thermodynamic relationships (e.g., Duffy and Anderson, 1989) and experimental results (Murase and Kushiro, 1977; Sato et al., 1989), Iwamori and Zhao (2000) calculated the seismic velocity structures from the predicted distribution of temperature, aqueous fluid, and melt. The results show that a remarkable low velocity zone (−6%) exists beneath the backarc region at depths of ~75–100 km in the mantle wedge. The velocity reduction is due partly to the presence of a relatively large amount of aqueous fluid and melt; this corresponds to the H_2O-rich regions beneath the backarc side in Fig. 6a.

This feature coincides well with the tomographic images based on P-wave velocity beneath NE Japan (Zhao et al., 1992), and also coincides well with recent finer tomographic images of the same region for both P- and S-waves (Nakajima et al., 2001). Fig. 8 displays the low S-wave velocity region (2% slower than the average) as a shaded region in the mantle wedge, and the distribution of *b*-values of the earthquake magnitude–frequency relationship from Wyss et al. (2001) and Hasegawa (2002). The low velocity region coincides

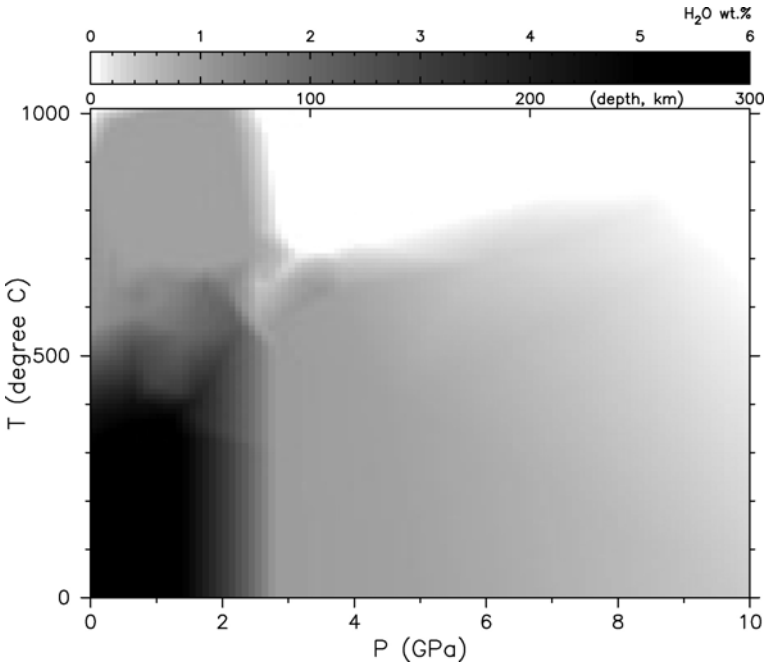

Fig. 5. Maximum content of H_2O in the solid phases of a basaltic system (mid-ocean ridge basalt composition), as a continuous function of pressure and temperature based on Schmidt and Poli (1998), reproduced from Iwamori (1998).

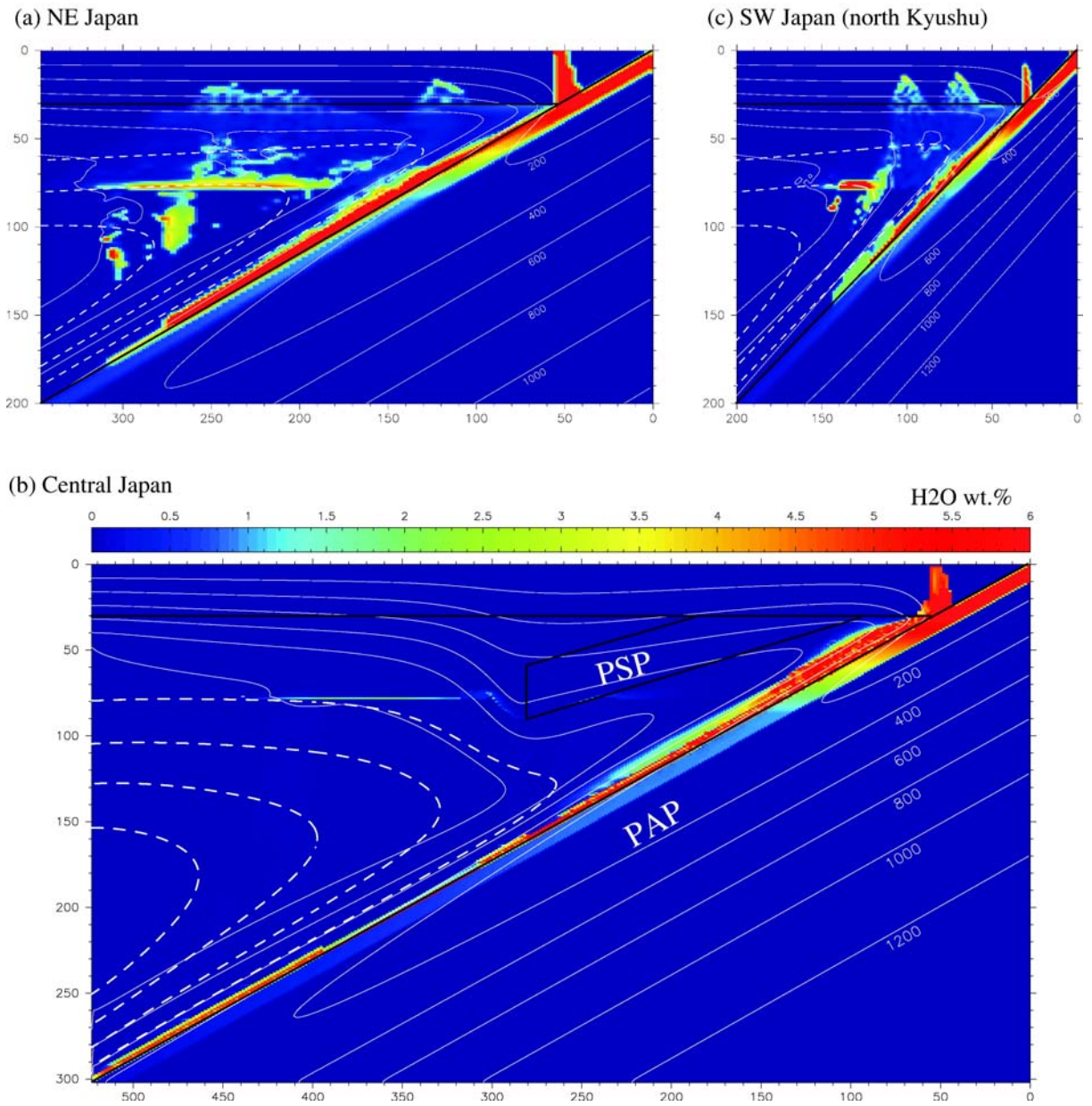

Fig. 6. Distribution of H_2O (total amount in each local bulk system, summing up H_2O in all the phases present in the local system) predicted by the numerical models for (a) northeast Japan reproduced from Iwamori and Zhao (2000), (b) central Japan reproduced from Iwamori (2000), (c) southwest Japan (north Kyushu) reproduced from Zhao et al. (2000). The two-dimensional cross sections are taken along the three dashed lines in Fig. 2. The common configurations are shown in Fig. 1. In each model (a) to (c), the arc crust is assumed to be 30 km thick. Also the oceanic crust is assumed to be 7 km thick in each figure, which is assumed to contain 6 wt.% H_2O initially and subducts from the upper right corner. The Moho and the interface between the subducting slab and the overlying mantle wedge are shown by thick solid lines. In (b), the Philippine Sea plate (labeled 'PSP') is modeled as a stagnant block extending perpendicular to the cross section (see text for the details), whereas the Pacific plate (labeled 'PAP') subducts from the upper right corner. The white lines indicate the isothermal contours with 200 °C interval. The white broken lines indicate the stream lines in the mantle wedge.

well with the H_2O-rich regions (i.e., rich in aqueous fluid and melt) in Fig. 6a. Also, a region with a high *b*-value at 140–150 km depth near the interface between the subducting slab and the overlying mantle wedge coincides with the breakdown point of serpentine in the model shown in Fig. 6a, where a thin 'red' layer just above the slab disappears. A high *b*-value means that smaller earthquakes occur more frequently, which in this

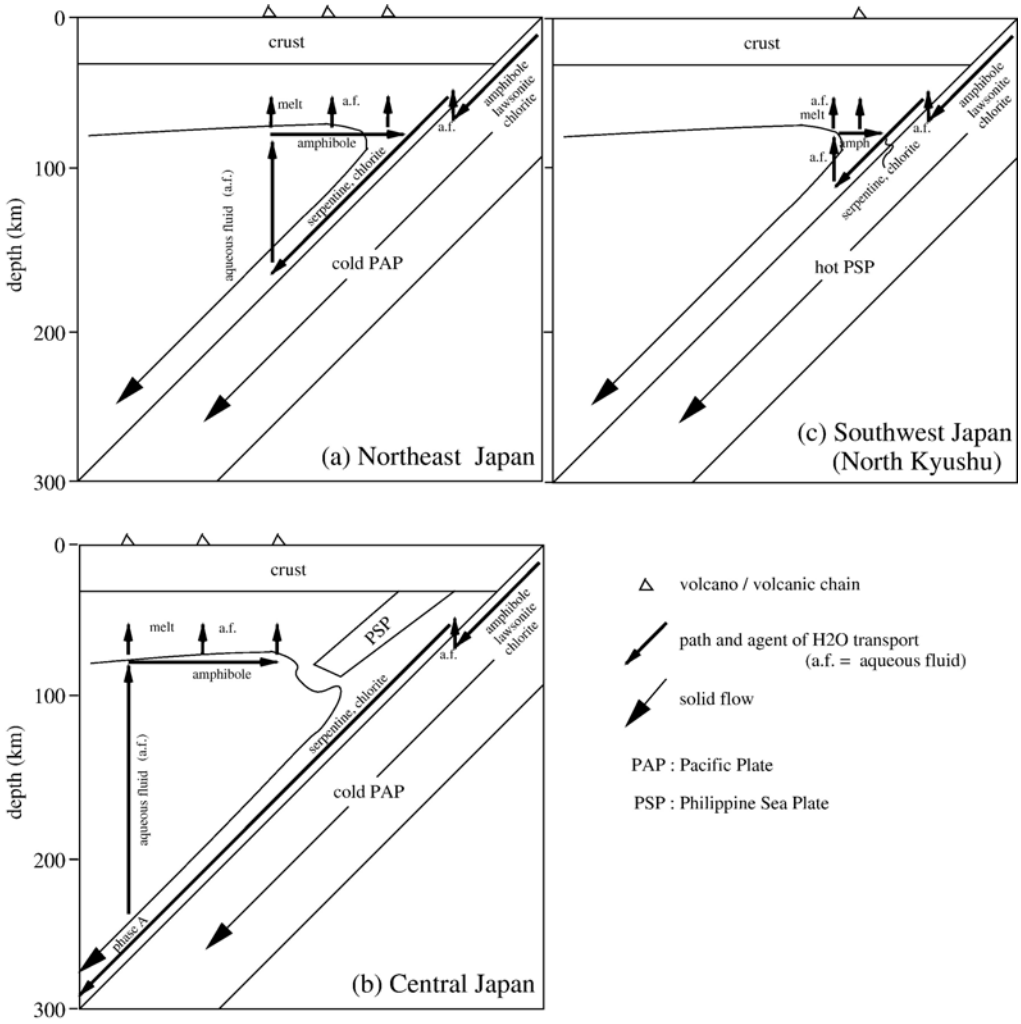

Fig. 7. Schematic figure showing transportation paths of H_2O and the transportation agents along the paths beneath (a) NE Japan, (b) central Japan, (c) SW Japan (north Kyushu), corresponding to Fig. 6a to c, respectively. Note that the subduction angle is not properly drawn in (a) and (b), for simplicity.

case is interpreted as a consequence of the presence of abundant aqueous fluid that increases pore pressure and reduces rock strength (Wyss et al., 2001), and is consistent with breakdown of serpentine at the depth.

In this model, the aqueous fluid released from the subducting slab is assumed to migrate via porous flow. The solubility of silicate components in the aqueous fluid at depth is probably high, since the P–T condition is close to or even above the second critical endpoint of 3.8 GPa and 1000 °C in the peridotite–H_2O system (Mibe et al., 2004; Kawamoto, 2006). Therefore, the liquid is expected to have a melt-like composition (rich in silicate components) and have a small dihedral angle that permits it to form an extensive liquid network (Shimizu and Takei, 2005), resulting in porous flow. Porous flow migration of such a liquid is supported by the seismic analyses used to detect the presence of fluid and pore geometry (Nakajima et al., 2005), as has been discussed.

If we assume that the fluid is transported through sparsely distributed cracks or channels, H_2O expelled from the subducting slab is not entirely trapped by serpentinite as it enters the mantle wedge. Iwamori and Zhao (2000) calculated such a case as a ‘disequilibrium model’, and show that a significant amount of aqueous fluid is supplied upwards straight from the subducting oceanic crust at depths shallower than 100 km. Consequently, a broad region beneath the forearc to volcanic front, where the depth of the Wadati–Benioff zone is shallower than 100 km, is predicted to exhibit a

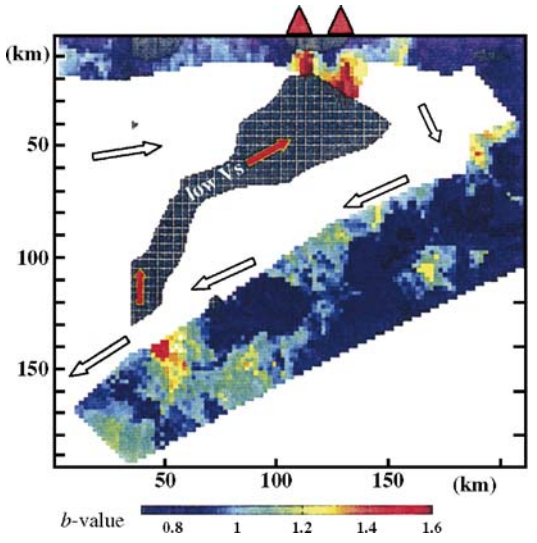

Fig. 8. Distribution of the low S-wave velocity region (slower than 2% than the average) as a shaded region in the mantle wedge, and distribution of *b*-value of earthquake magnitude–frequency relationship, which measures the ratio of small to large events, from Wyss et al. (2001) and Hasegawa (2002). White and red arrows indicate directions of solid flow and fluid flow in the mantle wedge, respectively (Wyss et al., 2001).

significant decrease in seismic velocity (e.g., a 6% decrease in V_P : see Fig. 1b and d of Iwamori and Zhao (2000) for the details). However, this is not the case beneath NE Japan. Therefore, the dehydration–hydration reactions during the migration of fluid from the slab and within the mantle wedge are thought to be close to equilibrium, although some of the components exhibiting a low diffusivity in solid might achieve only partial chemical equilibrium between the fluid and the solid.

4.2. Central Japan

In central Japan, in addition to subduction of the Pacific plate from the east, the overlapping subduction of the Philippine Sea plate occurs from the Sagami and Nankai troughs to the northwest (Figs. 2 and 3). While the volcanic chain in northeast Japan and the Izu–Ogasawara arc is located 80 to 150 km above the Wadati–Benioff zone of the subducted Pacific plate, the active volcanic chain in central Japan is located 170 to 300 km above the Wadati–Benioff zone, resulting in a deflection of the volcanic chain towards the backarc side (Fig. 3).

Iwamori (2000) modeled the transportation of H_2O and melting beneath central Japan for the cross-section A–B shown in Fig. 3, based on the plate configuration deduced from the seismic studies reported in Ishida (1992). In the cross-section, the Philippine Sea plate should have a velocity component perpendicular to the cross-section. However, the motion of the Philippine Sea plate is slower than that of the Pacific plate, and the subducted Philippine Sea plate is modeled as a stagnant block in the mantle wedge (a block labeled 'PSP' in Fig. 6b). In this case, a hot mantle material from the backarc is prevented from flowing into the corner region, resulting in slow thermal recovery of the subducting Pacific plate (e.g., 370 °C at a depth of 100 km, 550 °C at 200 km beneath central Japan, whereas 490 and 610 °C beneath northeast Japan) (Fig. 6a and b). Consequently, the dehydration reactions of serpentine are shifted deeper, resulting in melting far from the trench. The model result also indicates that H_2O is not entirely released even after dehydration of serpentine and chlorite, as phase-A is stable at this pressure and can transport a significant quantity of H_2O to a depth greater than 300 km (Fig. 7b). In this case, ~20% of the subducted water is transported to the deep mantle at a rate of 2.3×10^9 kg yr^{-1} per 1 km along the arc strike (Iwamori, 2000).

This is confirmed by plotting the geotherm along the subducting Pacific plate beneath central Japan with the stability fields of the hydrous phases (Fig. 9). Because of the very cold environment due to the double subducting plates, the geotherm (labeled 'central Japan' in Fig. 9) is very low. It passes mainly through the stability field of serpentine and phase A, without releasing all the H_2O near the 'choke point' around 6 GPa (e.g., Kawamoto et al., 1996), where the stability fields of hydrous minerals have a minimum temperature. On the other hand, the geotherm along the subducting Pacific plate beneath NE Japan (labeled 'NE Japan' in Fig. 9) is at a slightly higher temperature suggesting that most of the H_2O is released below 6 GPa, as in Fig. 6a.

4.3. Southwest Japan

In contrast with the cold environment in central Japan, subduction of the young Shikoku basin (27 to 15 Ma, Fig. 2) significantly affects the fluid processes beneath Shikoku, Chugoku, and northern Kyushu in southwest Japan. The model prediction for such a case with the subduction of a young (20 Ma) slab is shown in Fig. 6c (reproduced from Zhao et al., 2000). The young subducted slab promotes dehydration reactions at depths shallower than those beneath northeast and central Japan. Fig. 6c shows that the H_2O-rich regions with aqueous fluid and melt are distributed beneath the volcanic front to forearc region, rather than beneath the backarc.

The tomographic image (V_P) beneath northern Kyushu, an across-arc section through Kuju volcano, shows a low V_P region extending beneath the volcanic

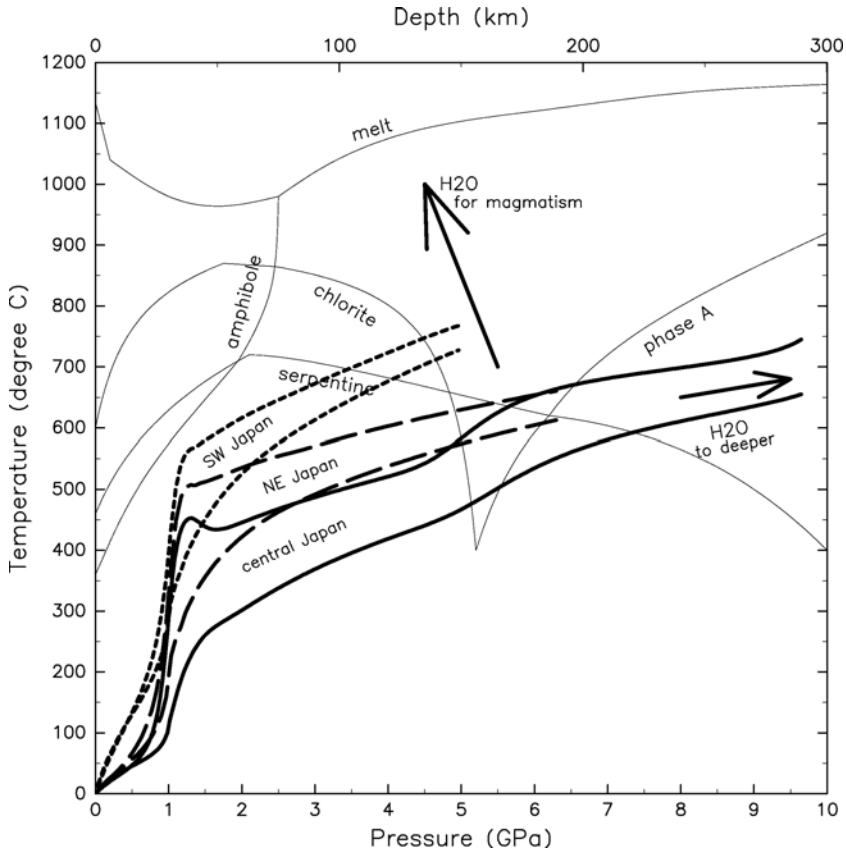

Fig. 9. Stability fields of the major hydrous phases, and geotherms along the subducting slab–wedge interface and within the mantle wedge above the slabs (~6 km away from the interface) calculated in the three models shown in Fig. 6. The geotherms labeled 'central Japan' (thick solid lines) correspond to those along the subducting Pacific plate beneath central Japan. Of the two lines, the one that passes at lower temperature corresponds to the geotherm along the slab–wedge interface, while the line at higher temperature corresponds to the geotherm within the mantle wedge above the slabs (~6 km away from the interface). The geotherms labeled 'NE Japan' (broken lines) correspond to those along the subducting Pacific plate beneath northeast Japan. The geotherms labeled 'SW Japan' (dotted lines) correspond to those along the subducting Philippine Sea plate beneath north Kyushu (SW Japan).

front (beneath which the depth of Wadati–Benioff zone is about 100 km) to the forearc region (see Fig. 2 of Zhao et al. (2000)). The pattern of fluid distribution in the model is consistent with the low V_P region in the tomographic image and distribution of the nonvolcanic deep tremors caused by fluids (Obara, 2002). Therefore, the aqueous fluid is thought to be present mainly beneath the volcanic front to forearc regions in northern Kyushu and Shikoku due to subduction of the warm Shikoku basin. This is confirmed again by plotting the geotherm along the subducting Shikoku Basin, labeled 'SW Japan' in Fig. 9, although the relative sequence of dehydration and transportation agents of H_2O remains the same as in NE Japan (Fig. 7a and c).

In central to southern Kyushu, where a relatively cold plate subducts (older than 50 Ma, Fig. 2), the low-V_P region and the dense seismicity in the forearc region disappear (Zhao et al., 2000). Instead, a low-V_P region appears beneath the volcanic front to the backarc side. Since the other subduction parameters such as subduction velocity and angle are similar for northern and southern Kyushu, it is concluded that the age of the subducting plate controls the fluid processes in the region.

5. Summary and implications for global circulation of H_2O

The three cases from NE, central and SW Japan arcs clarify the following points. First, an aqueous fluid released from the subducting oceanic crust forms a serpentinite layer in the mantle wedge just above the subducting slab, maintaining a condition close to equilibrium in terms of dehydration–hydration reactions

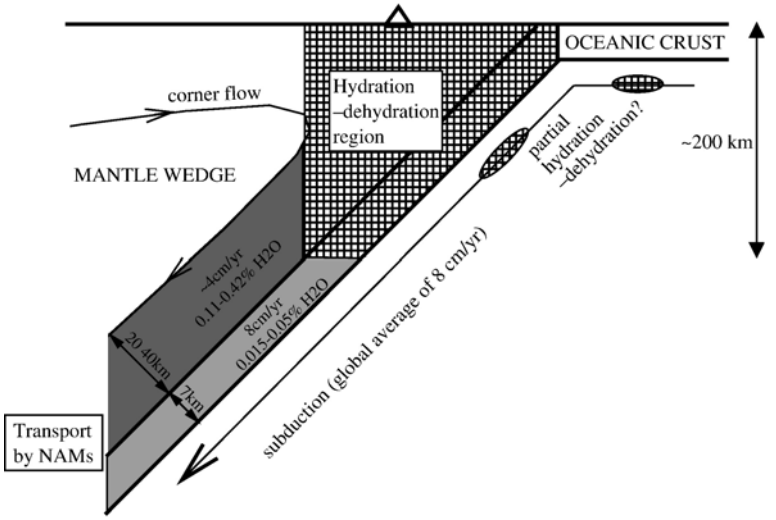

Fig. 10. Schematic illustration showing the existence of two different domains within subduction zones in terms of transportation of H_2O: (1) at relatively shallow depths (e.g., shallower than 200 km), the mantle wedge undergoes significant hydration from the slab and dehydration of major hydrous minerals (a hatched domain labeled 'Hydration–dehydration region'), and (2) at depths greater than the domain (1), the nominally anhydrous mineral phases (NAMs) in both subducting oceanic crust and the overlying mantle wedge can carry a significant amount of H_2O to the deep mantle (shaded domains labeled 'Transport by NAMs'). The amount of H_2O transported to the deep mantle (i.e., transition zone) is estimated based on the maximum H_2O content in the nominally anhydrous minerals, considering the geometry and the velocities as are shown in the figure (see text for the details).

during aqueous fluid migration. Second, most of the H_2O is transported to a depth where serpentine and chlorite in the serpentinite layer break down. This depth depends on the thermal structure of the slab. The dehydration depth is greater for the older plate beneath the Japan arcs, ~150 km for subduction of the Pacific plate (130 Ma old) in northeast Japan (Fig. 7a), and shallower for subduction of the Shikoku basin (~20 Ma old, Fig. 7c). Third, beneath central Japan, the subducted Philippine Sea plate overlapping the subducted Pacific plate causes a slow thermal recovery of the latter (Fig. 9), resulting in dehydration and melting far from the trench (Fig. 6b). Consequently, the volcanic chain in the region deflects towards the backarc side. In this exceptionally cold environment even among the subduction zones, H_2O is transported down to a depth greater than 300 km by phase-A, after the breakdown of serpentine (Fig. 7b). The transportation of H_2O, as modeled in this study, is rather different from the conventional view that aqueous fluid and melt are transported directly upward to the volcanic front (e.g., Tatsumi, 1989).

This also has an important implication for the evolution of mantle convection and the thermal history of the Earth. In the past when the mantle potential temperature was high, H_2O may not have been transported down as effectively into the deep mantle (hot–dry regime) due to the higher temperatures of subducting slabs. As the Earth cools down in future, more H_2O may get into the deep mantle (cold–wet regime), which will reduce the viscosity and melting temperature of the mantle. In this case, the Rayleigh number might not decrease as much as we expect only from the temperature decrease. This negative feedback may stabilize and prolong the convective motion of the Earth, using effectively the limited heat sources within the Earth. In this sense, the present-day Earth may be at the beginning of the transition from a hot–dry regime to a cold–wet regime, as is suggested by the existence of the very cold environment in central Japan, where a leakage of H_2O to the deep mantle occurs.

Considering that the Pacific plate is one of the oldest subducting plates in the world, in most of the subduction zones (except for a very cold subduction zone such as the central Japan arc), dehydration of the oceanic crust and the overlying mantle wedge (the serpentinite layer) is expected to occur at depths shallower than ~200 km as is seen in NE and SW Japan. The aqueous fluid generated at these depths ascends to cause melting in the central portion of the mantle wedge which triggers arc magmatism. The effective dehydration of the subducting slab is consistent with the previous result based on the composition of the plume-influenced mid-ocean ridge basalts as a recycled subducted material (Dixon et al.,

2002). However, it should be noted that even after the completion of dehydration of major hydrous mineral phases in the subducting materials, nominally anhydrous phases can retain H_2O to carry it to the deep mantle. Forneris and Holloway (2003) estimate that a coesite-bearing eclogite as a dehydrated oceanic crust can still contain 0.015 to 0.05 wt.% H_2O without major hydrous phases. The mantle wedge undergoes significant hydration from the slab and dehydration of major hydrous minerals above 200 km depth (mainly between 100 and 150 km); however it can still carry about 0.11 to 0.42 wt.% H_2O (Fig. 4b) to the deep mantle, as is schematically shown in Fig. 10. The thickness of the downgoing mantle flow above the subducting slab is estimated to be 20–40 km based on the results shown in Fig. 6.

Using a total length of convergent plate boundaries and a global average velocity of subduction (3.7×10^7 m and 8 cm/yr, Reymer and Schubert (1984)), a global average thickness (7 km) of the oceanic crust (White et al., 1992), and a mean density of rocks of 3×10^3 kg m^{-3}, the calculated flux of H_2O transported by nominally anhydrous phases to the deep mantle is on the order of 1.1×10^{11} to 7.8×10^{11} kg yr^{-1}. The maximum estimate of 7.8×10^{11} kg yr^{-1} is based on the maximum H_2O content of the upper mantle assemblage of Hirschmann et al. (2005) shown in Fig. 4b (dotted line) with the thickness of the downgoing mantle wedge of 40 km in Fig. 10, while the minimum estimate of 1.1×10^{11} kg yr^{-1} is based on that of Bolfan-Casanova (2005) shown in Fig. 4b (dashed line) with the thickness of 20 km.

Seno and Yamanaka (1996) and Yamasaki and Seno (2003) pointed out that double seismic zones observed in some sub-ducting slabs may represent serpentine dehydration reactions, indicating partial hydration of the subducting oceanic lithosphere. Based on double-difference high-resolution tomography, Zhang et al. (2004) find a high V_P/V_S region within the subducting slab beneath NE Japan, but do not find evidence for abundant serpentinite within the subducting plate. Therefore, the quantity of H_2O in the subducting oceanic mantle may be small and highly localized. The model presented here neglects this water from the estimation of the influx, although it needs to be quantitatively estimated in future.

The minimum estimate of the influx of H_2O, 1.1×10^{11} kg yr^{-1}, is comparable to the out-flow of H_2O from the mantle associated with magmatism at mid-ocean ridges and hotspots of 1.2×10^{11} kg yr^{-1} (Ito et al., 1983). In this case, the regassing and degassing are balanced and achieve a (quasi-)steady state, as is reproduced by the box model of parameterized mantle convection and water cycling (McGovern and Schubert, 1989).

If the influx of H_2O is close to the maximum estimate, 7.8×10^{11} kg yr^{-1}, then the excess influx of 6.6×10^{11} kg yr^{-1} must be stored in the Earth's interior. Based on Jambon and Zimmermann (1990), the mass of H_2O within the Earth's interior is estimated to be 6.4×10^{21} kg H_2O or 4.5 times of the current ocean mass, which is less than the quantity of H_2O that can be stored in the Earth's mantle (Table 1). Therefore, the excess of influx may be accumulated in the Earth's mantle. However, the transport of 6.6×10^{11} kg yr^{-1} H_2O into the solid Earth should cause a detectable decrease in the abundance of surface water. Complete suction occurs in 2.1 Gyr assuming the constant rate, which is not supported by the current understanding of the history of ocean mass and crustal growth based on constancy of freeboard since the Archean (e.g., Reymer and Schubert, 1984). This unbalance becomes greater if a significant amount of H_2O is contained in the oceanic lithospheric mantle as was discussed, which makes the maximum estimate of the influx of H_2O even more unrealistic. In any case, the maximum H_2O content of the upper mantle assemblage at the base of the mantle wedge and in the subducting slab affects greatly the global water circulation, which remains to be constrained.

Acknowledgments

The author thanks T. Iidaka and T. Kawamoto for their discussions and help, and G.C. Richard and P. Ulmer for their constructive review, and A.C. Simon for the editorial handling and proofreading of the manuscript.

References

Arcay, D., Tric, E., Doin, M.-P., 2005. Numerical simulations of subduction zones — effect of slab dehydration on the mantle wedge dynamics. Phys. Earth Planet. Inter. 149, 133–153.

Bell, D.R., Rossman, G.R., 2003. Hydroxide in olivine: a quantitative determination of the absolute amount and calibration of the IR spectrum. J. Geophys. Res. 108, 2105, doi:10.1029/2001JB000679.

Bird, P., 2003. An updated digital model of plate boundaries. Geochem. Geophys. Geosyst. 4, 1027, doi:10.1029/2001GC000252.

Bolfan-Casanova, N., 2005. Water in the Earth's mantle. Mineral. Mag. 69, 229–257.

Bolfan-Casanova, N., Keppler, H., Rubie, D.C., 2000. Water partitioning between nominally anhydrous minerals in the MgO–SiO_2–H_2O system up to 24 GPa: implications for the distribution of water in the Earth's mantle. Earth Planet. Sci. Lett. 182, 209–221.

Bose, K., Ganguly, J., 1995. Experimental and theoretical studies of the stabilities of talc, antigorite and phase A at high pressures with

applications to subduction processes. Earth Planet. Sci. Lett. 136, 109–121.
Davies, J.H., Stevenson, D.J., 1992. Physical model of source region of subduction zone volcanics. J. Geophys. Res. 97, 2037–2070.
DeMets, C., Gordon, R.G., Argus, D.F., Stein, S., 1990. Current plate motions. Geophys. J. Int. 101, 425–478.
Dixon, J.E., Leist, L., Langmuir, C., Schilling, J.-G., 2002. Recycles dehydrated lithosphere observed in plume-influenced mid-ocean-ridge basalt. Nature 420, 385–389.
Duffy, T.S., Anderson, D.L., 1989. Seismic velocities in mantle minerals and the mineralogy of the upper mantle. J. Geophys. Res. 98, 20005–20013.
Dziewonski, A.M., Anderson, D.L., 1981. Preliminary reference Earth model. Phys. Earth Planet. Inter. 25, 297–356.
Forneris, J.F., Holloway, J.R., 2003. Phase equilibria in subducting basaltic crust: implications for H_2O release from the slab. Earth Planet. Sci. Lett. 214, 187–201.
Furukawa, Y., 1993. Depth of the decoupling plate interface and thermal structure under arcs. J. Geophys. Res. 98, 20005–20013.
Hasegawa, A., 2002. Seismic imaging underneath northeast Japan. Kagaku (Science) 72, 194–203 (in Japanese).
Hirose, K., 1997. Melting experiments on lherzolite KLB-1 under hydrous conditions and generation of high-magnesian andesitic melts. Geology 25, 42–44.
Hirschmann, M.M., Aubaud, C., Withers, A.C., 2005. Storage capacity of H_2O in nominally anhydrous minerals in the upper mantle. Earth Planet. Sci. Lett. 236, 167–181.
Honda, S., Yoshida, T., 2005. Application of the model of small-scale convection under the island arc to the NE Honshu subduction zone. Geochem. Geophys. Geosyst. 6, Q01002, doi:10.1029/2004GC000785.
Inoue, T., 1994. Effect of water on melting phase relations and melt composition in the system Mg_2 SiO_4–$MgSiO_3$–H_2O up to 15 GPa. Phys. Earth Planet. Inter. 85, 237–263.
Inoue, T., Yurimoto, H., Kudoh, Y., 1995. Hydrous modified spinel, $Mg_{1.75}SiH_{0.5}O_4$: a new water reservoir in the mantle transition region. Geophys. Res. Lett. 22, 117–120.
Iidaka, T., Mizoue, M., Nakamura, I., Tsukada, T., Sakai, K., Kobayasi, M., Haneda, T., Hashimoto, S., 1990. The upper boundary of the Philippine Sea plate beneath the western Kanto region estimated from S–P-converted wave. Tectonophysics 179, 321–326.
Ishida, M., 1992. Geometry and relative motion of the Philippine Sea plate and Pacific plate beneath the Kanto-Tokai District, Japan. J. 12Geophys. Res. 97, 489–513.
Ito, E., Harris, D.M., Anderson, A.T., 1983. Alteration of oceanic crust and geologic cycling of chlorine and water. Geochim. Cosmochim. Acta 47, 1613–1624.
Iwamori, H., 1991. Zonal structure of Cenozoic basalts related to mantle upwelling in southwest Japan. J. Geophys. Res. 96, 6157–6170.
Iwamori, H., 1992. Degree of melting and source composition of Cenozoic basalts in southwest Japan: evidence for mantle upwelling by flux melting. J. Geophys. Res. 97, 10983–10995.
Iwamori, H., 1998. Transportation of H_2O and melting in subduction zones. Earth Planet. Sci. Lett. 160, 65–80.
Iwamori, H., 2000. Deep subduction of H_2O and deflection of volcanic chain towards backarc near triple junction due to lower temperature. Earth Planet. Sci. Lett. 181, 41–46.
Iwamori, H., 2004. Phase relations of peridotites under H_2O-saturated conditions and ability of subducting plates for transportation of H_2O. Earth Planet. Sci. Lett. 227, 57–71.
Iwamori, H., Zhao, D., 2000. Melting and seismic structure beneath the northeast Japan arc. Geophys. Res. Lett. 27, 425–428.
Jambon, A., Zimmermann, J.L., 1990. Water in oceanic basalts: evidence for dehydration of recycled crust. Earth Planet. Sci. Lett. 101, 323–331.
Kamiya, S., Kobayashi, Y., 2000. Seismological evidence for the existence of serpentinized wedge mantle. Geophys. Res. Lett. 27, 819–822.
Katayama, I., Hirose, K., Yurimoto, H., Nakashima, S., 2003. Water solubility in majoritic garnet in subducting oceanic crust. Geophys. Res. Lett. 30, 2155, doi:10.1029/2003GL018127.
Kawamoto, T., 2004. Hydrous phase stability and partial melt chemistry of H_2O-saturated KLB-1 peridotite up to the uppermost lower mantle conditions. Phys. Earth Planet. Inter. 143–144, 387–395.
Kawamoto, T., 2006. Hydrous phases and water transport in the subducting slab. In: Keppler, H., Smyth, J.R. (Eds.), Water in nominally anhydrous minerals. Reviews in Mineral. Geochem. 62, Mineral. Soc. Am. and Geochem. Soc. Am., pp. 273–289.
Kawamoto, T., Holloway, J., 1997. Melting temperature and partial melt chemistry of H_2O-saturated mantle peridotite to 11 giga-pascals. Science 276, 240–243.
Kawamoto, T., Herving, R.L., Holloway, J.R., 1996. Experimental evidence for a hydrous transition zone in the early Earth's mantle. Earth Planet. Sci. Lett. 142, 587–592.
Kohlstedt, D.L., Keppler, H., Rubie, D.C., 1996. Solubility of water in the α, β and γ phases of $(Mg,Fe)_2SiO_4$. Contrib. Mineral. Petrol. 123, 345–357.
Komabayashi, T., Omori, S., Maruyama, S., 2004. Petrogenetic grid in the system MgO–SiO_2–H_2O up to 30 GPa, 1600 C: applications to hydrous peridotite subducting into the Earths deep interior. J. Geophys. Res. 109, B03206, doi:10.1029/2003JB002651.
Kimura, J., Tateno, M., Osaka, I., 2005. Geology and geochemistry of Karasugasen lava dome, Daisen-Hiruzen volcano group, southwest Japan. Isl. Arc 14, 115–136.
Kondo, H., Kaneko, K., Tanaka, K., 1998. Characterization of spatial and temporal distribution of volcanoes since 14 Ma in the Northeast Japan arc. Bull. Volcanol. Soc. Japan 43, 173–180.
Lu, R., Keppler, H., 1997. Water solubility in pyrope to 100 kbar. Contrib. Mineral. Petrol. 129, 35–42.
Litasov, K., Ohtani, E., 2003. Stability of various hydrous phases in CMAS pyrolite–H_2O system up to 25 GPa. Phys. Chem. Miner. 30, 147–156.
Litasov, K., Ohtani, E., Langenhorst, F., Yurimoto, H., Kubo, T., Kondo, T., 2003. Water solubility in Mg-perovskite and water storage capacity in the lower mantle. Earth Planet. Sci. Lett. 211, 189–203.
Matsubara, M., Obara, K., Kasahara, K., 2005. High-V_P/V_S zone accompanying non-volcanic tremors and slow slip events beneath the Tokai region, central Japan. EOS, Transactions. American Geophysical Union. T33B-0539.
McGovern, P.J., Schubert, G., 1989. Thermal evolution of the Earth: effects of volatile exchange between atmosphere and interior. Earth Planet. Sci. Lett. 96, 27–37.
Mibe, K., Kanzaki, M., Kawamoto, T., Matsukage, K.N., Fei, Y., Ono, S., 2004. Second critical endpoint in peridotite–H_2O system and its bearing on the magmatism in subduction zones. AGU Fall Meeting. abstract: V11C-07.
Mierdel, K., Keppler, H., 2004. The temperature dependence of water solubility in enstatite. Contrib. Mineral. Petrol. 148, 305–311.
Murakami, M., Hirose, K., Yurimoto, H., Nakashima, S., Takafuji, N., 2002. Water in Earth's lower mantle. Science 295, 1885–1887.
Murase, T., Kushiro, I., 1977. Compressional wave velocity in partially molten peridotite at high pressures. Carnegie Inst. Wash. Year Book, vol. 78, pp. 559–562.

Nakajima, J., Matsuzawa, T., Hasegawa, A., Zhao, D., 2001. Three-dimensional structure of V_P, V_S and V_P/V_S beneath northeastern Japan: implications for arc magmatism and fluids. J. Geophys. Res. 106, 21843–21857.

Nakajima, J., Takei, Y., Hasegawa, A., 2005. Quantitative analysis of the inclined low-velocity zone in the mantle wedge of northeastern Japan: a systematic change of melt-filled pore shapes with depth and its implications for melt migration. Earth Planet. Sci. Lett. 234, 59–70.

Nakamura, M., Yoshida, Y., Zhao, D., Yoshikawa, K., Takayama, H., Aoki, G., Kuroki, H., Yamazaki, T., Kasahara, J., Kanazawa, T., Sato, T., Shiobara, H., Shimamura, H., Nakanishi, A., 2002. Three-dimensional P and S wave velocity structure beneath Central Japan. Papers Meteorol. Geophys. 53, 1–28.

Nakanishi, I., 1980. Precursors to ScS phases and dipping interface in the upper mantle beneath southwestern Japan. Tectonophysics 69, 1–35.

Obara, K., 2002. Nonvolcanic deep tremor associated with subduction in southwest Japan. Science 296, 1679–1681.

Okino, K., Shimakawa, Y., Nagaoka, S., 1994. Evolution of the Shikoku Basin. J. Geomagn. Geoelectr. 46, 463–479.

Ono, S., 1998. Stability limits of hydrous minerals in sediment and mid-ocean ridge basalt compositions: implications for water transport in subduction zones. J. Geophys. Res. 103, 18253–18267.

Rauch, M., Keppler, H., 2002. Water solubility in orthopyroxene. Contrib. Mineral. Petrol. 143, 525–536.

Reymer, A., Schubert, G., 1984. Phanerozoic addition rates to the continental crust and crustal growth. Tectonics 3, 63–77.

Rüpke, L.H., Morgan, J.P., Hort, M., Connolly, J.A.D., 2004. Serpentine and the subduction zone water cycle. Earth Planet. Sci. Lett. 223, 17–34.

Sato, H., Sacks, I.S., Murase, T., 1989. The use of laboratory velocity data for estimating temperature and partial melt fraction in the low velocity zone: comparison with heat flow and electrical conductivity studies. J. Geophys. Res. 95, 5689–5704.

Schmidt, M., Poli, S., 1998. Experimentally based water budgets for dehydrating slabs and consequences for arc magma generation. Earth Planet. Sci. Lett. 163, 361–379.

Schubert, D., Turcotte, D.L., Olson, P., 2001. Mantle Convection in the Earth and Planets. Cambridge Univ. Press, Cambridge.

Seno, T., Yamanaka, Y., 1996. Double seismic zones, compressional deep trench-outer rise events, and superplumes. In: Bebout, G.E., Scholl, D.W., Kirby, S.H., Platt, J.P. (Eds.), Subduction: top to bottom. Geophys. Monogr. 96, Am. Geophys. Union, Washington DC, pp. 347–355.

Seno, T., Stein, S., Gripp, A.E., 1993. A model for the motion of the Philippine Sea plate consistent with Nuvel-1 and geological data. J. Geophys. Res. 98, 17941–17948.

Shimizu, I., Takei, Y., 2005. Temperature and compositional dependence of solid–liquid interfacial energy: application of the Cahn–Hilliard theory. Physica, B + C 362, 169–179.

Skogby, H., 1994. OH incorporation in synthetic clinopyroxene. Am. Mineral. 79, 240–249.

Smyth, J.R., 1987. β–Mg_2SiO_4: a potential host for water in the mantle? Am. Mineral. 72, 1051–1055.

Tamura, Y., Tatsumi, Y., Zhao, D., Kido, Y., Shukuno, H., 2002. Hot fingers in the mantle wedge: new insights into magma genesis in subduction zones. Earth Planet. Sci. Lett. 197, 105–116.

Tatsumi, Y., 1989. Migration of fluid phases and genesis of basalt magmas in subduction zones. J. Geophys. Res. 94, 4697–4707.

Tokuyama, H., 1995. Origin and development of the Philippine Sea. In: Tokuyama, H., Shcheka, S.A., Isezaki, N., et al. (Eds.), Geology and Geophysics of the Philippine Sea. Terrapub, Tokyo, pp. 155–163.

Turcotte, D.L., Schubert, G., 1982. Geodynamics: Applications of Continuum Physics to Geological Problems. John Wiley, New York.

van Kenken, P.E., Kiefer, B., Peacock, S.M., 2002. High-resolution models of subduction zones: implications for mineral dehydration reactions and the transport of water into the deep mantle. Geochem. Geophys. Geosyst. 3, 1056, doi:10.1029/2001GC000256.

White, R.S., McKenzie, D., O'Nions, R.K., 1992. Oceanic crustal thickness from seismic measurements and rare earth element inversions. J. Geophys. Res. 97, 19683–19715.

Whitford-Stark, J.L., 1987. A survey of Cenozoic volcanism on mainland Asia. Geol. Soc. Amer. Spec. Paper 213 (74 pp.).

Withers, A.C., Wood, B.J., Carroll, M.R., 1998. The OH content of pyrope at high pressure. Chem. Geol. 147, 161–171.

Wyss, M., Hasegawa, A., Nakajima, J., 2001. Source and path of magma for volcanoes in the subduction zone of northeastern Japan. Geophys. Res. Lett. 28, 1819–1822.

Yamasaki, T., Seno, T., 2003. Double seismic zone and dehydration embrittlement of the subducting slab. J. Geophys. Res. 108, 2212, doi:10.1029/2002JB001918.

Zhang, H., Thurber, C.H., Shelly, D., Ide, S., Beroza, G.C., Hasegawa, A., 2004. High-resolution subducting-slab structure beneath northern Honshu, Japan, revealed by double-difference tomography. Geology 32, 361–364.

Zhao, D., Hasegawa, A., 1993. P wave tomographic imaging of the crust and upper mantle beneath the Japan islands. J. Geophys. Res. 98, 4333–4353.

Zhao, D., Hasegawa, A., Horiuchi, S., 1992. Tomographic imaging of P and S wave velocity structure beneath northeastern Japan. J. Geophys. Res. 97, 19909–19928.

Zhao, D., Asamori, K., Iwamori, H., 2000. Seismic structure and magmatism of the young Kyushu subduction zone. Geophys. Res. Lett. 27, 2057–2060.

Zhao, Y.-H., Ginsberg, S.B., Kohlstedt, D.L., 2004. Solubility of hydrogen in olivine: dependence on temperature and iron content. Contrib. Mineral. Petrol. 147, 155–161.